

PAPER

Development of two-stage solidification technology for implementing micro structures with liquid magnetic polymer and solid magnetic anisotropic polymer

To cite this article: Fu-Ming Hsu and Weileun Fang 2014 *J. Micromech. Microeng.* **24** 095024

View the [article online](#) for updates and enhancements.

Related content

- [A review of the hybrid techniques for the fabrication of hard magnetic microactuators based on bonded magnetic powders](#)
M Pallapa and J T W Yeow
- [Magnetic and viscoelastic response of elastomers with hard magnetic filler](#)
E Yu Kramarenko, A V Chertovich, G V Stepanov et al.
- [Removable fast package technology for MEMS devices](#)
Chia-Min Lin, Wen-Chih Chen and Weileun Fang



IOP | ebooks™

Bringing you innovative digital publishing with leading voices to create your essential collection of books in STEM research.

Start exploring the collection - download the first chapter of every title for free.

Development of two-stage solidification technology for implementing micro structures with liquid magnetic polymer and solid magnetic anisotropic polymer

Fu-Ming Hsu¹ and Weileun Fang^{1,2}

¹ Power Mechanical Engineering, National Tsing Hua University, Hsinchu, Taiwan

² Institute of NanoEngineering and MicroSystems, National Tsing Hua University, Hsinchu, Taiwan

E-mail: fang@pme.nthu.edu.tw

Received 6 May 2014, revised 27 June 2014

Accepted for publication 7 July 2014

Published 19 August 2014

Abstract

This study presents two-stage solidification technology for fabricating micromagnetic polymer composite (MPC, polymer with magnetic particles) structures. In this process, ultra-violet (UV)-light polymer curing is used for the first stage of MPC solidification. The surface of the MPC structure is solidified in this step. Moreover, thermal polymer curing is employed for the second stage of MPC solidification. The second stage of curing was mainly for the body solidification of the MPC. The distribution of magnetic particles in MPC can be specified by applying a magnetic field during the second solidification process. Based on the presented process technologies, microstructures with liquid MPC (NdFeB particles of different wt% in liquid polymer), isotropic solid MPC and anisotropic solid MPC have been demonstrated. Microdevices with liquid MPC embedded in solid micro balls and thin layers are also demonstrated. Various tests are performed to characterize the magnetic properties of the fabricated micro MPC structures. Measurements show that the fabricated solid MPC has reasonable coercivity, as compared with bulk materials. However, the remanence and the saturation magnetization still need to be improved.

Keywords: two-stage solidification, UV curing, thermal curing, magnetic polymer composites (MPC)

(Some figures may appear in colour only in the online journal)

1. Introduction

Permanent magnetic films can find various applications in MEMS devices. Many approaches have been reported to deposit permanent magnet materials on MEMS devices [1–4]. For instance, sputter deposition and electroplating are two popular approaches to prepare hard magnet films. However, the annealing temperature is a critical concern for the sputtered and electroplated magnetic films. A post-annealing treatment is required for the crystallization of sputtered or electroplated magnetic films in order to improve the coercivity [5, 6]. In general, such a high annealing temperature

may lead to thermal residual stresses or damage to the already deposited films.

Preparing magnetic film using magnetic polymer composites (MPC, polymer with magnetic particles) is another promising process technique. The process used to implement the MPC film is a low temperature approach. The high performance magnetic film can be achieved by using powders of a strong magnet (such as NdFeB [3, 4, 7–10]). Thermal polymerization and photochemical polymerization (especially ultraviolet (UV)-light curing) are two common approaches to preparing MPC structures [3, 4, 11, 12]. The low temperature batch preparation of MPC is achieved through a

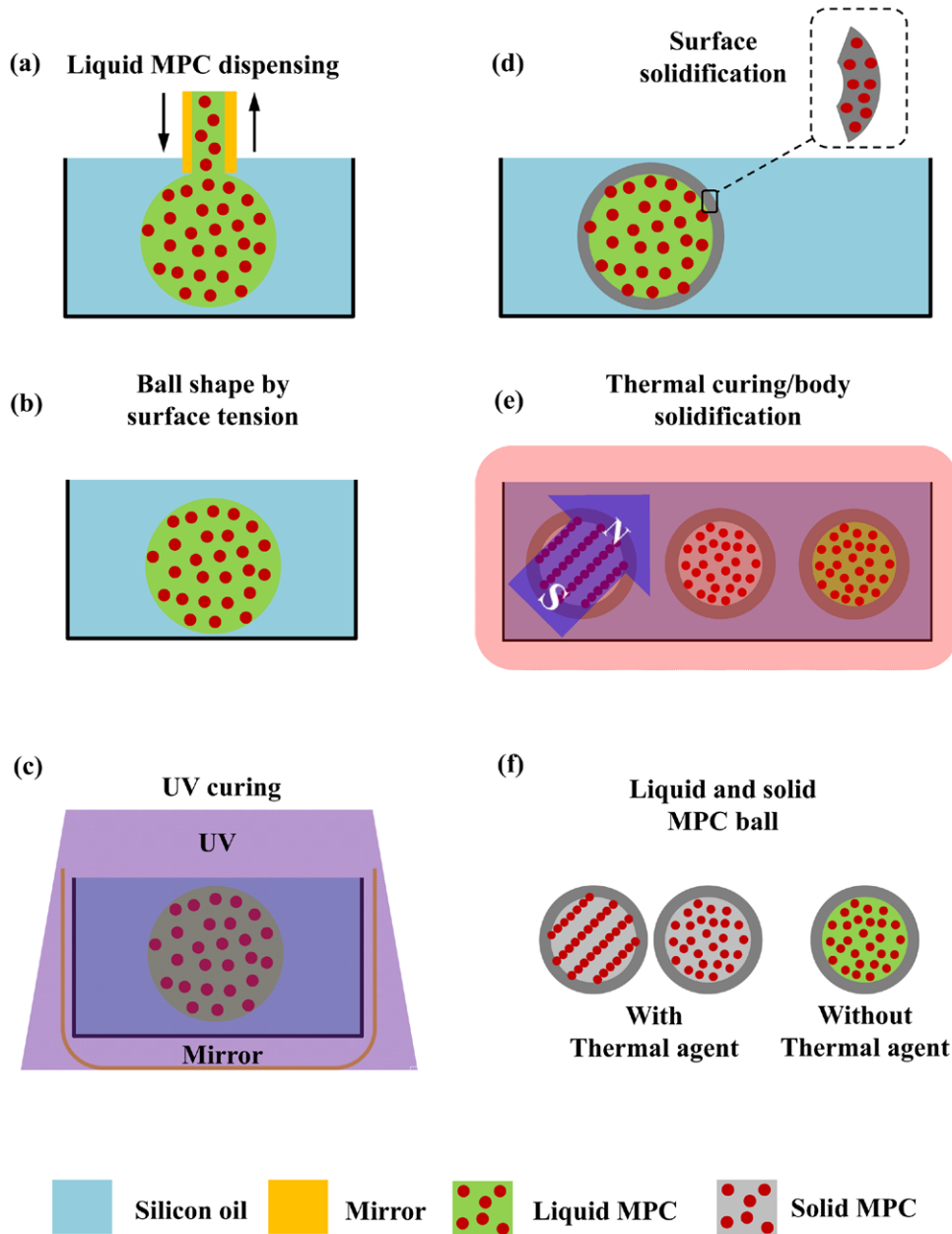


Figure 1. Fabrication process flow of the two-stage polymer solidification technology to fabricate the discrete micro balls with liquid MPC, solid isotropic MPC and solid anisotropic MPC.

photochemical approach to polymer mixing with low wt% magnetic particles and photocurable carrier matrix [11, 12]. Moreover, the polymer mixed with magnetic particles and thermal curing agent is solidified by low temperature (even room temperature) heating [3, 4]. However, control of the magnetization direction remains a challenge for both thermal and photochemical polymerization processes [3, 4, 12]. In addition, the additives absorb incoming light, which further influences the curing depth of polymer composites for the photochemical approach [13].

The magnetic properties of MPC is influenced by the alignment and distribution of magnetic particles in polymer [7, 10]. The magnetic particles spread in fluid and could become redistributed to form chain-like structures by an externally applied magnetic field. This phenomenon is the

so-called magnetorheological effect [14, 15]. The shape of the chain-like structure in fluid is affected by the dipole motion and attraction between magnetic powders. Due to the magnetorheological effect, material properties, such as optical [16], electro [17], magnetic [18], thermal [19] and mechanical [20], could be changed from isotropic to anisotropic by the magnetic field. For instance, this characteristic has been employed in [20] to change the stiffness of a structure with a magnetic fluid. Note that the characteristics of the magnetorheological effect could be influenced by the carrier fluid viscosity, size, shape, magnetic of particles, volume fraction of particles in MPC and magnetic field intensity [18].

This study will demonstrate a two-stage low temperature solidification process [21, 22] used to fabricate micro

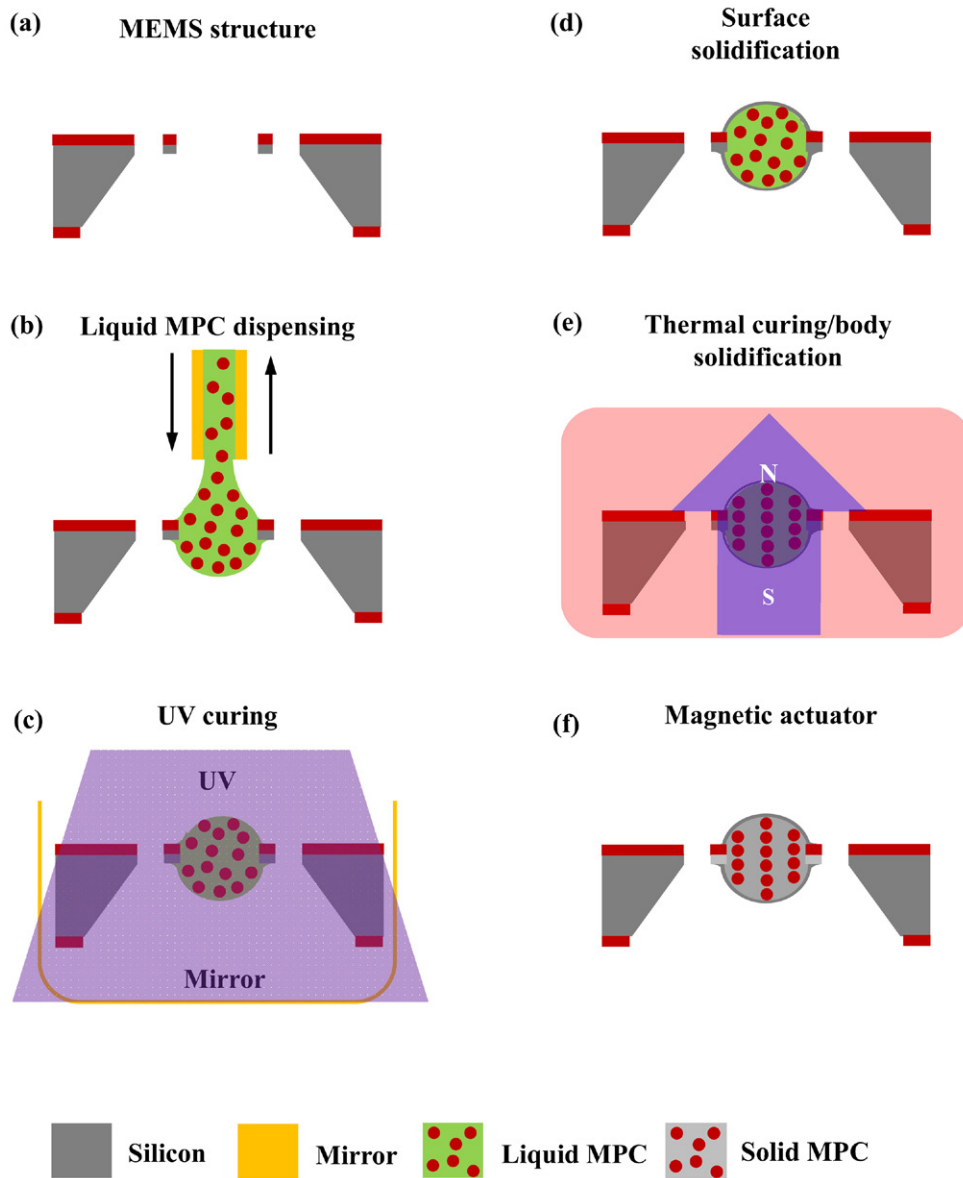


Figure 2. Fabrication process flow to integrate a magnetic anisotropic MPC ball with a suspended MEMS structure.

MPC structures. Thus the micro MPC structures can be implemented and further integrated with MEMS devices on substrate. In contrast to existing MEMS-integrated MPC processes, this study employs the photochemical (UV-light) approach for the first stage of polymer curing to solidify the surface of the MPC structures. Thus, the shape of the MPC structures has been determined by the solidified surface. The MPC inside the solidified surface remains in liquid phase. After that, the second stage of polymer solidification is performed with thermal curing. Meanwhile, anisotropic MPC could be achieved by applying an external magnetic field during the second stage of curing. Based on the presented process technologies, micromagnetic structures with (1) liquid MPC, (2) isotropic solid MPC, and (3) anisotropic solid MPC, can be fabricated. In other words, micro MPC structures with different magnetic properties can be achieved by using the presented low temperature two-stage solidification process technology.

2. Concept and fabrication processes

This study presents the two-stage solidification process technology on UV-curable polymer. The process technology is further employed to implement the anisotropic MPC. Figure 1 shows the concept and process flow of the two-stage polymer solidification technology. As shown in figure 1(a), a liquid phase MPC was prepared using UV curable polymer with specified wt% magnetic powders. Note that NdFeB magnetic powder is used in this study. The wt% of magnetic powder changes the magnetic properties of the MPC. As shown in figure 1(b), the liquid phase MPC was dispensed into liquid by a hydraulic dispensing system [23]. The first stage of polymer curing was then performed by using UV light, as shown in figure 1(c). After that, the surface of the MPC ball was solidified by UV curing, as depicted in figure 1(d). Finally, the second stage of thermal curing was performed on the MPC ball with a

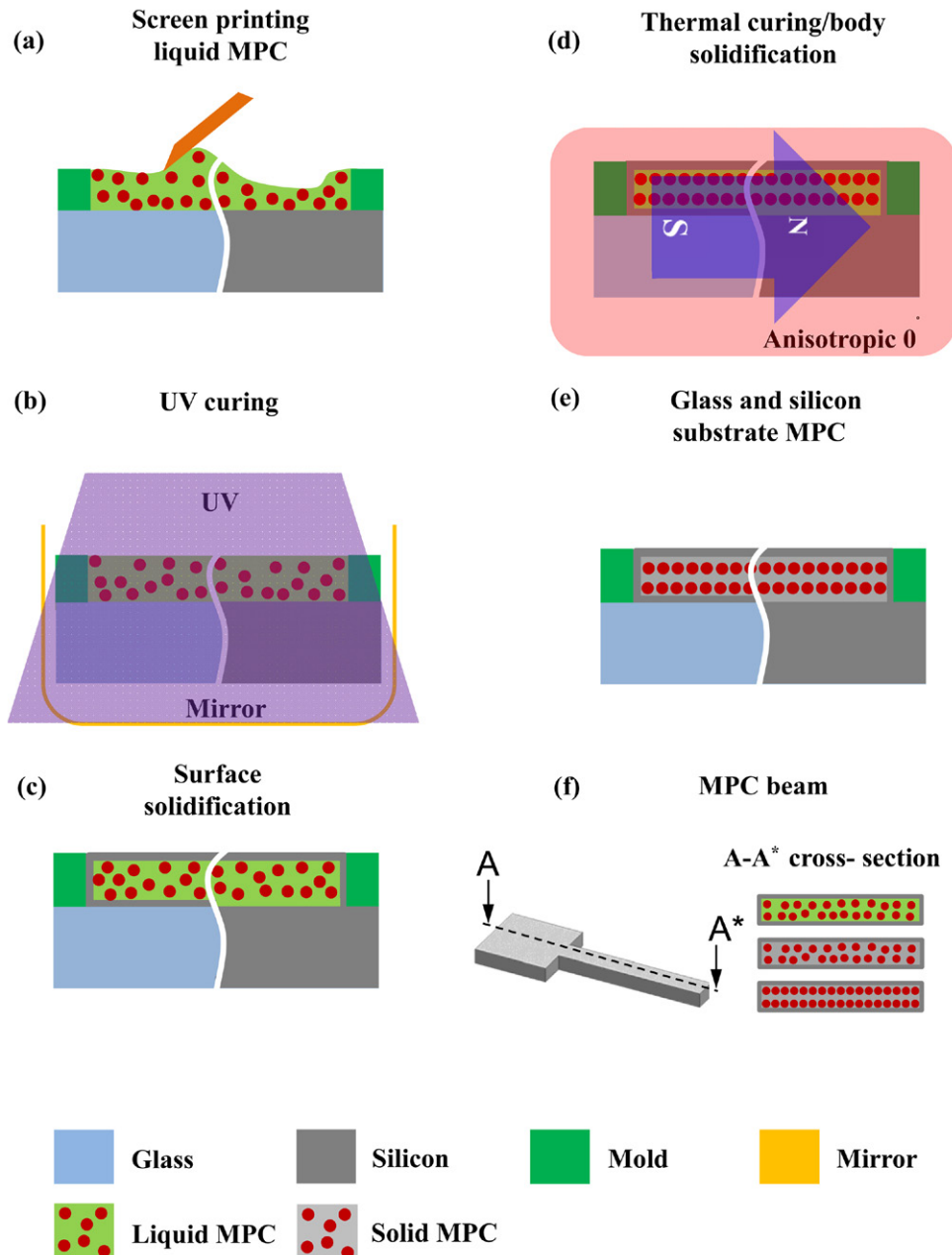


Figure 3. Schematic concept and process flow to implement MPC layers on silicon or glass substrates.

solidified surface through the rising temperature, as shown in figure 1(e). The second stage of curing was mainly for the body solidification of the MPC. The magnetic field could be applied to the MPC ball during the second stage of curing. Thus, as shown in the left-hand illustration in figure 1(f), a solidified MPC ball with anisotropic magnetic properties was achieved. However, the MPC ball has isotropic magnetic properties when no magnetic field is applied during thermal curing, as the middle illustration shows in figure 1(f). Moreover, to achieve the second stage body solidification of MPC, a thermal curing agent needs to be added to liquid polymer. This study also implements a micro ball with liquid MPC encapsulated by the solidified surface, as shown in the right-hand illustration in figure 1(f). In this case, the thermal curing agent is not added to the liquid polymer.

The concept in figure 1 can be further extended to implement the magnetic anisotropic MPC on suspended MEMS devices, as shown in figure 2. Figures 2(a), (b) depicts the dispensing of liquid MPC onto a suspended MEMS structure [24]. As shown in figures 2(c), (d), the first stage of surface solidification of liquid MPC was achieved by using UV curing. After that, the second stage of body solidification of liquid MPC was realized by using thermal curing, as illustrated in figures 2(e), (f). Meanwhile, the anisotropy of the MPC was also defined by an external magnetic field in this step. Thus, the integration of a suspended MEMS device with the magnetic anisotropic MPC structure was implemented. In addition, the concept in figure 1 can also be extended to realize the magnetic anisotropic MPC on silicon substrate shown in figure 3. As illustrated in figure 3(a), the liquid phase MPC was patterned by screen printing on silicon or glass substrate.

Similarly, the first stage of UV curing was employed for MPC surface solidification, as shown in figures 3(b), (c). Note that the bottom surface of liquid MPC can only be solidified on a transparent glass substrate, as displayed in figure 3(c). Moreover, the second stage of thermal curing for body solidification of MPC was performed as shown in figure 3(d). The magnetic anisotropy of the MPC was also defined at this stage by applying a magnetic field during the curing process. As illustrated in figure 3(e), the magnetic anisotropic MPC thin layer was realized on substrate. However, the second stage of body solidification of MPC cannot be achieved for the polymer with no thermal curing agent. Such a structure will consist of liquid MPC encapsulated by the solidified surface, as depicted in figure 3(c). Moreover, the thin MPC layers in figure 3(e) could be removed from the substrate. Thus, the discrete micro components formed by the magnetic anisotropic or isotropic MPC, or even liquid MPC, were achieved, as shown in figure 3(f).

3. Fabrication results

To demonstrate the feasibility of the present fabrication process technologies, various different magnetic anisotropic MPCs have been fabricated and integrated. In these case studies, commercially available neodymium (NdFeB) was employed as the permanent magnetic powder. The NdFeB powder with particle sizes of near $1\mu\text{m}$ were prepared by ball mill grinding at a rotational rate of 50rpm for 48h. The average grain size of the NdFeB powder is near 100 nm. Commercially available polyurethane (PU) resin was employed to prepare the polymer MPC. The liquid magnetic polymer composites were prepared by using a homogenizer system (KK-250S, KURABO). While preparing the liquid MPC, a specific weight percentage (10, 30, 50 wt%) of NdFeB powder was mixed with PU (including the photo-initiator). The photo-initiator contains a mixture of chemicals that can be activated by UV light with wavelength near 400 nm. Thus, the first stage of surface solidification of liquid MPC by UV curing can be achieved.

The UV transmittance of MPC determines the thickness of the first stage of polymer solidification [9]. This study prepared six different solidified MPC samples ($15\mu\text{m}$ thick) with NdFeB weight fractions of 0 to 50 wt% between two transparent microscope slides. The UV transmittance of MPC was then characterized using these samples through the test setup shown in figure 4(a). The UV transmittance (for wavelength of near 400 nm) of MPCs with NdFeB of different weight-fractions can be identified under a high-resolution optical microscope, as depicted in figure 4(b). The measured profiles from a spectrometer (Mission Peak Optics MP100-M) in terms of different contents of NdFeB powder are plotted in figure 4(c). The results indicate that the UV transmittance is 46% (UV intensity dropped from 3500 count to 1600 count) for the MPC with 0 wt% NdFeB (i.e. pure resin). As the wt% of NdFeB increased from 0 wt% to 20 wt%, the UV transmittance decreased to 30%. The UV transmittance becomes only 4% as the NdFeB weight fraction increased to 50 wt%. In this study, the UV curing for the first stage of surface

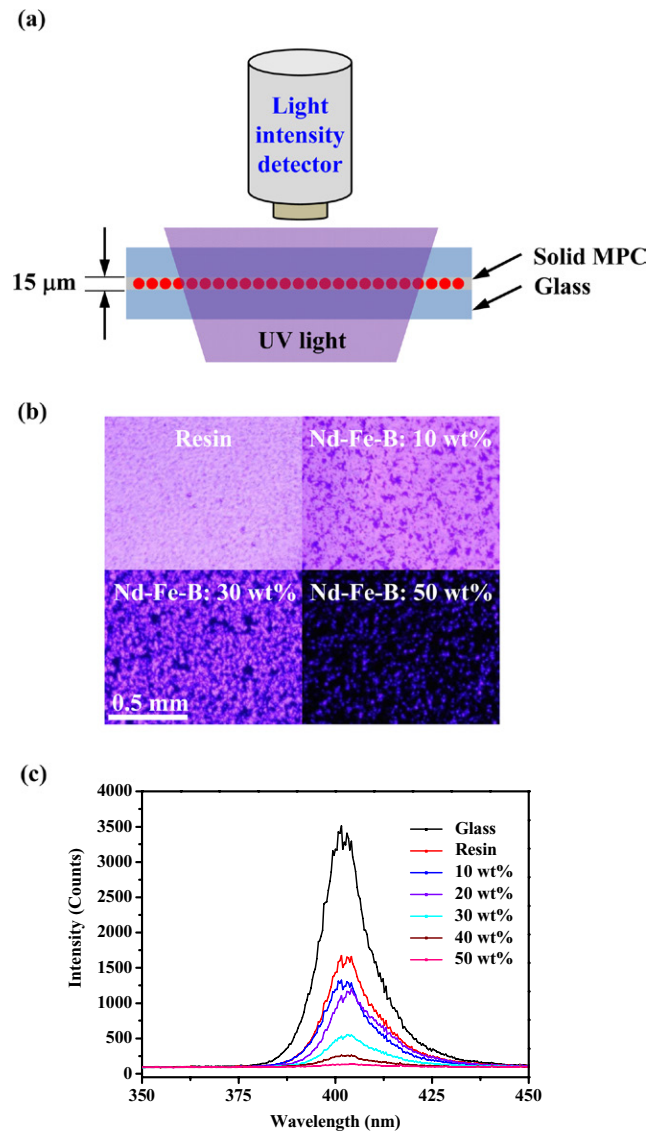


Figure 4. UV transmittance of MPC: (a) schematic diagram of the test setup; (b) optical photographs of resin with different weight fraction of NdFeB powders; and (c) measurement results of the optical spectrometer.

solidification of MPC has the same intensity of 60 mW cm^{-2} with a fixed curing time of 30 s. Thus, the surface thickness of the solidified MPC will vary with the wt% of NdFeB. Moreover, the second stage of body solidification of MPC was achieved in this study by thermal curing at room temperature for 24 h. A higher thermal curing temperature could reduce the curing time, yet residual stresses of the solidified MPC would be a concern.

The micrograph in figure 5(a) shows the cross sections of typical surface-solidified MPC balls fabricated by the processes indicated in figure 1(a)–(d). The liquid polymer of 10 wt% and 15 wt% NdFeB powder were respectively used to fabricate these two balls of $3000\mu\text{m}$ diameter. The solidification surface thicknesses of these two MPC balls are $694\mu\text{m}$ and $216\mu\text{m}$, respectively, after UV curing. Figure 5(b) further summarizes the solidification surface thicknesses d of the MPC ball for liquid polymer of different wt% of NdFeB

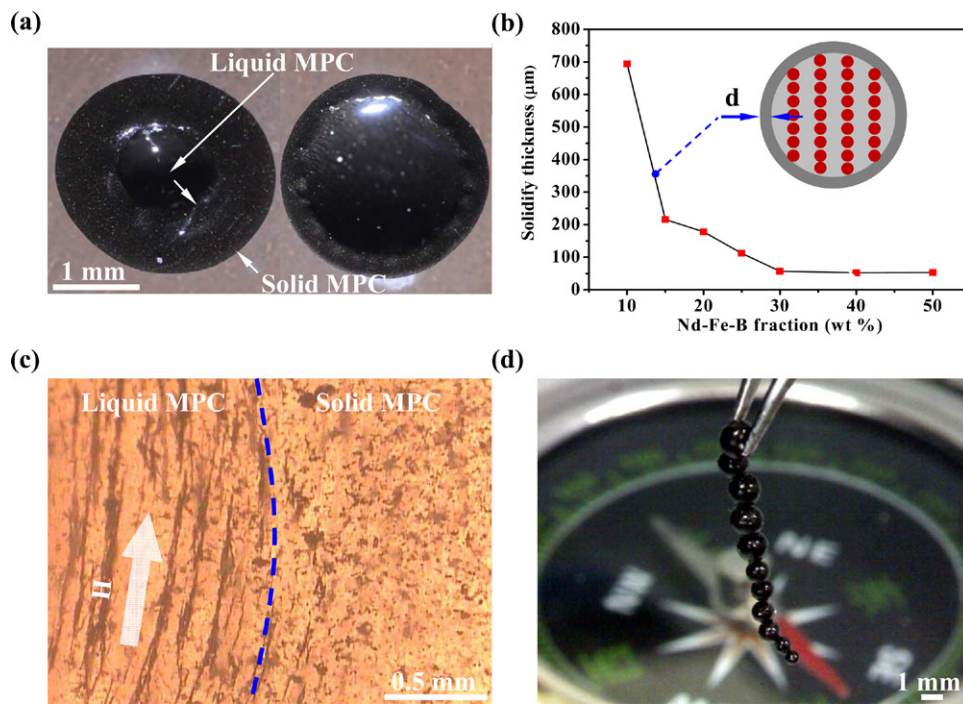


Figure 5. Typical fabrication results of discrete MPC balls: (a) the cross-section view of a surface-solidified MPC ball with 10 wt% NdFeB powder; (b) solidification thickness of the MPC ball varying with the weight fraction NdFeB powder; (c) zoom-in micrograph of the interface between the liquid and solid MPC shown in figure 5(a); and (d) optical image showing the attraction of fully solidified MPC balls with diameters ranging from 500 μm to 3200 μm.

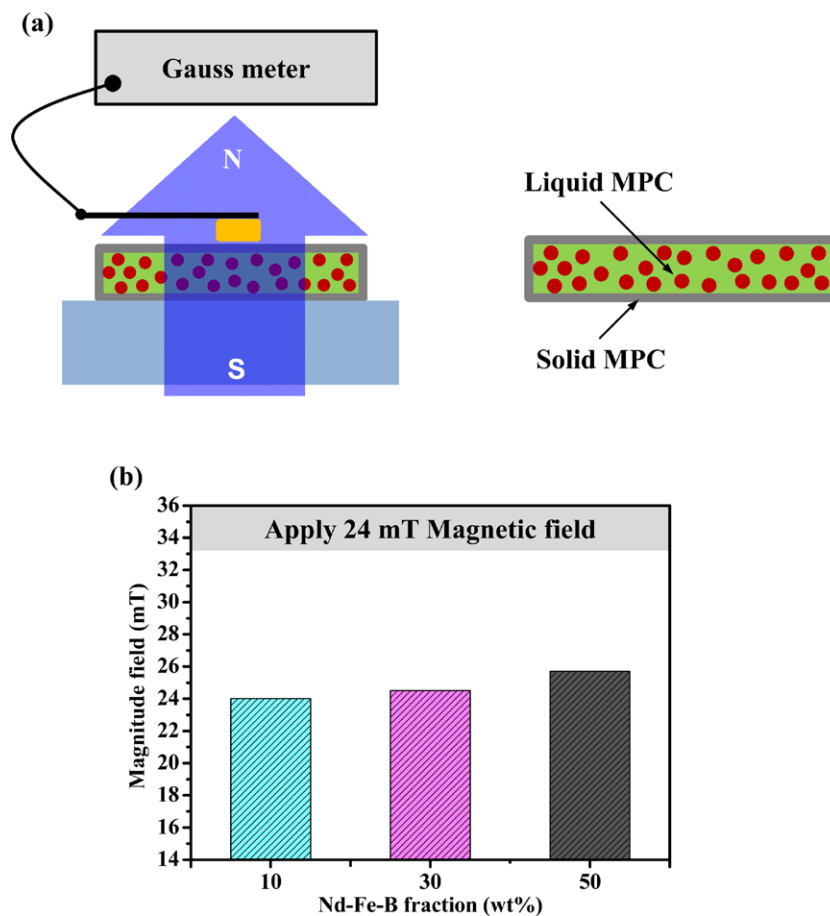


Figure 6. Measurements of the magnetic shielding effect of the MPC structure after the first stage of curing: (a) measurement setup; and (b) measurement results with different NdFeB contents under a 24-mT magnetic field.

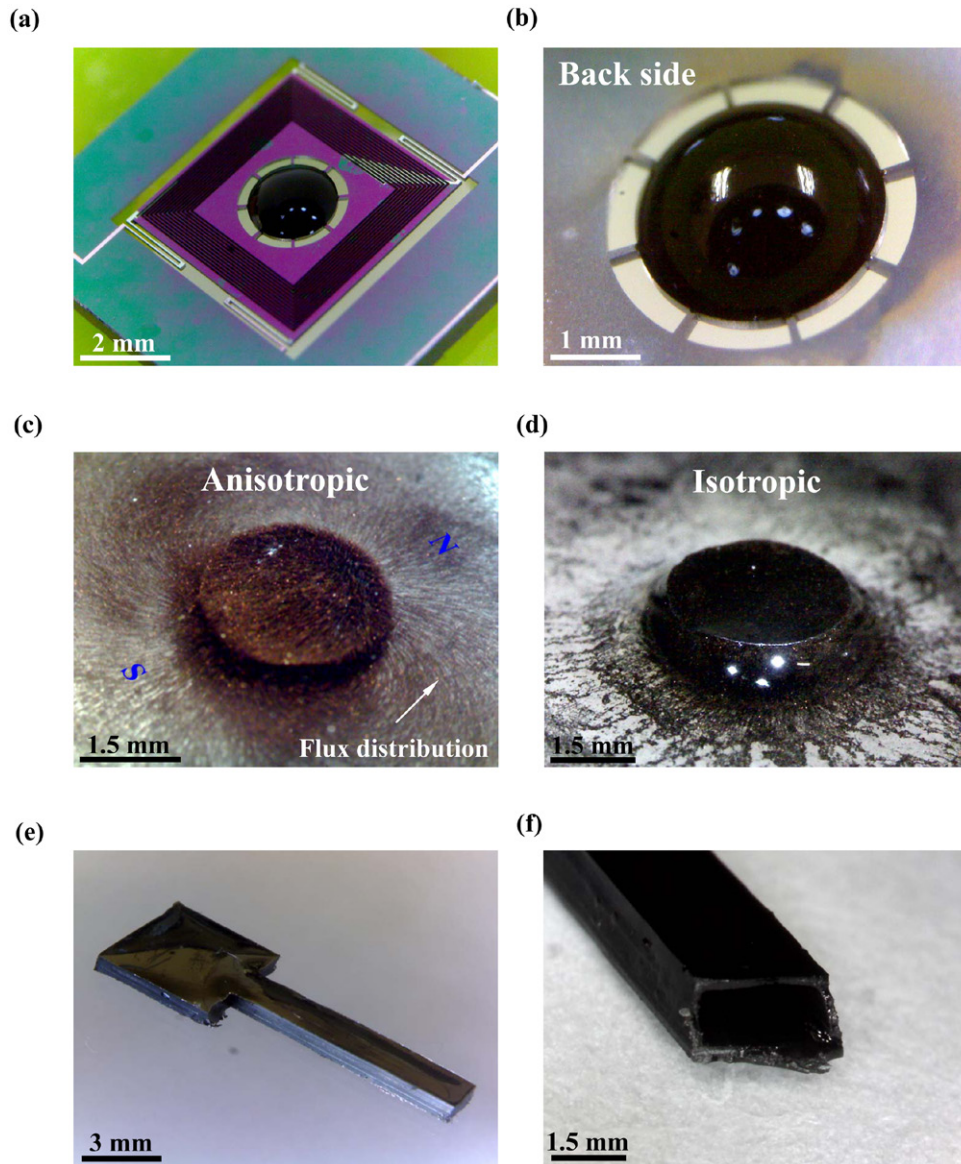


Figure 7. Typical fabrication results of the MPC structure implemented on silicon and glass substrates: (a), (b) integration of a solid magnetic anisotropic MPC ball on a suspended MEMS position stage; (c), (d) the visualized magnetic distribution (through magnetic powders) of fully-solidified magnetic anisotropic and isotropic MPC layers on a glass substrate; (e) a discrete micro structure with liquid MPC encapsulated inside the solidified surface, the structure parted from the glass substrate after the first stage curing; and (f) the cross section of the discrete component in figure 7(e).

powder. The variation of solidified surface thickness is due to the influence of UV transmittance, as discussed in figure 4. As the NdFeB powder exceeds 30 wt%, the solidification surface thickness of a MPC ball converges to $50\mu\text{m}$. The zoom-in micrograph in figure 5(c) further indicates the surface solidified MPC ball in figure 5(a). The NdFeB powder randomly distributed on the solidified surface is observed. Moreover, the liquid polymer inside the solidified surface contains NdFeB powder grains that are properly aligned by an external magnetic field (as indicated in figure 1(e)). Figure 5(d) demonstrates the attraction of fully solidified magnetic anisotropic MPC balls fabricated using the processes in figure 1. The diameter of these MPC balls ranges from $500\mu\text{m}$ to $3200\mu\text{m}$. The magnetic field applied on the MPC balls during the second stage of curing was 450 mT.

While applying magnetic fields to implement the magnetic anisotropic MPC structure during the second stage of curing, the magnetic shielding effect of the already solidified surface in the first stage of curing would be a concern. Note that the first stage solidified surface was formed by the isotropic MPC. Thus, the magnetic shielding effect of the MPC structure after the first stage of surface curing was characterized by using a Gauss meter (F W Bell Model 6010), as shown in figure 6(a). In this test, the sample ($10000\mu\text{m}$ in diameter and $3000\mu\text{m}$ in thickness) was prepared on transparent glass substrate using the processes shown in figure 3. The Gauss meter and the magnet were placed at a fixed distance during the shielding effect test. The magnetic field on top of the MPC layer was detected by the Gauss meter, and thus the magnetic shielding by the MPC layer was determined. A magnetic flux of 24 mT

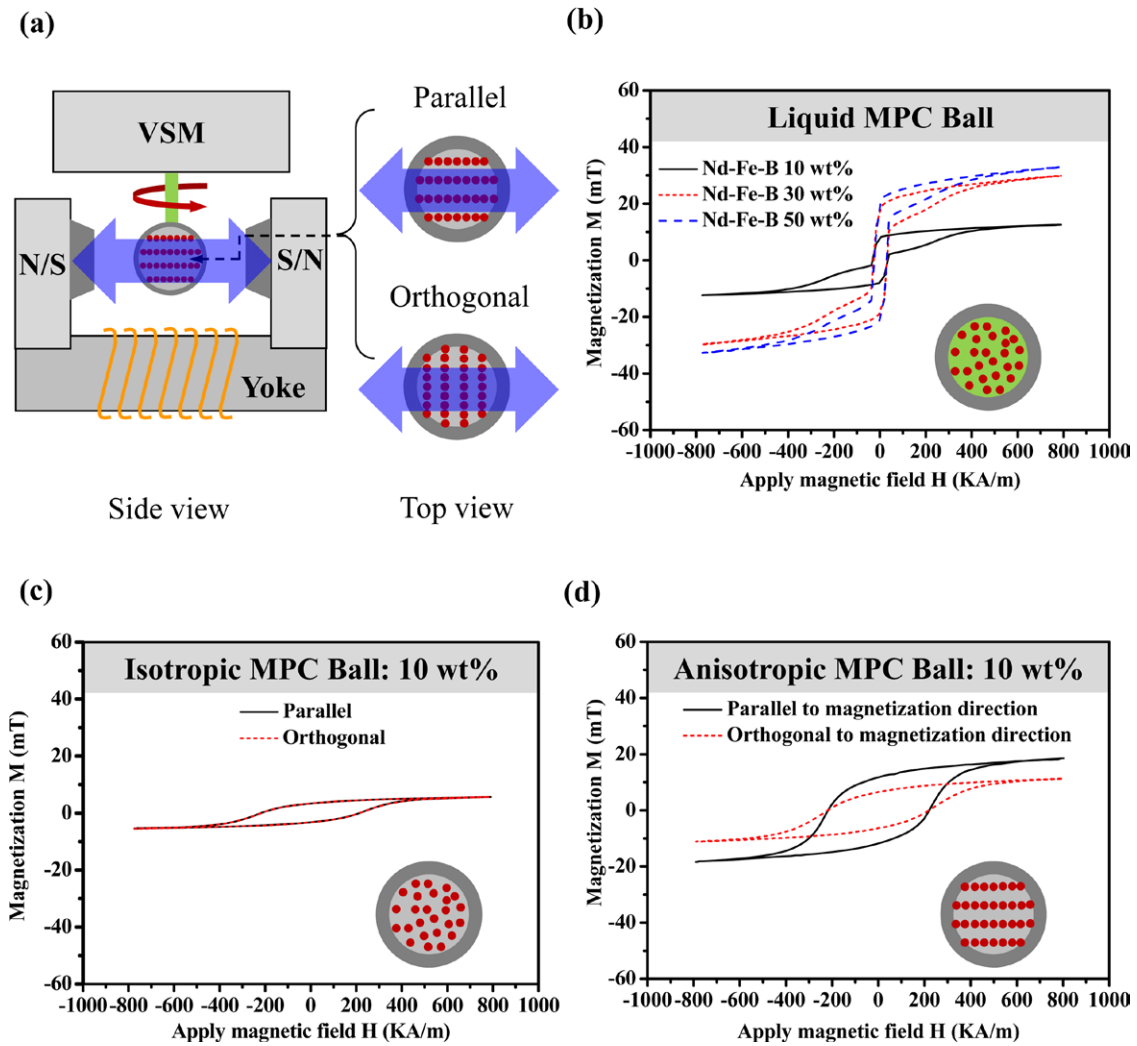


Figure 8. Measurements of the hysteresis loop ($M-H$ curve) of magnetic balls: (a) measurement setup of the VSM, and the measurement results for discrete magnetic balls with (b) liquid MPC of 10, 30 and 50 wt% NdFeB particles; (c), (d) solid magnetic isotropic and anisotropic MPCs of 10 wt% NdFeB particles measured in two orthogonal directions (apply magnetic field: $\pm 800 \text{ kA m}^{-1}$).

Table 1. The measured saturation magnetization, remanence and coercivity for the three types of micro balls (shown in figure 1(f)) with NdFeB particles of 10–50 wt%.

MPC	10			30			50		
	Liquid	Isotropic	An-isotropic	Liquid	Isotropic	An-isotropic	Liquid	Isotropic	An-isotropic
Saturation mag. Ms, (mTesla)	8.5	3.7	12	20	11.2	21.1	22	18.4	34.5
Remanence Br, (mTesla)	5.9	1.6	7.2	14	6.2	10	15	11.2	14
Coercivity Hci, (kA m ⁻¹)	~37	~280	~37	~37	~280	~37	~37	~280	~37

was measured without any MPC shielding. The measurement results summarized in figure 6(b) indicate that no magnetic shielding effect has occurred. Thus, the NdFeB particles could be aligned by the applied magnetic field to form the anisotropic MPC.

The micrograph in figure 7(a) shows the integration of a solid magnetic anisotropic MPC ball with a suspended MEMS position stage. The zoom-in micrograph in figure 7(b)

displays the shape of the MPC ball at the backside of the MEMS stage. This device was implemented using the processes shown in figure 2. The micrograph in figure 7(c) shows a single fully solidified magnetic anisotropic MPC layer (3000 μm in diameter and 500 μm in thickness) on a glass substrate. This device was implemented using the processes shown in figures 3(a)–(d). The distribution of surrounding magnetic particles indicates the anisotropic magnetic field.

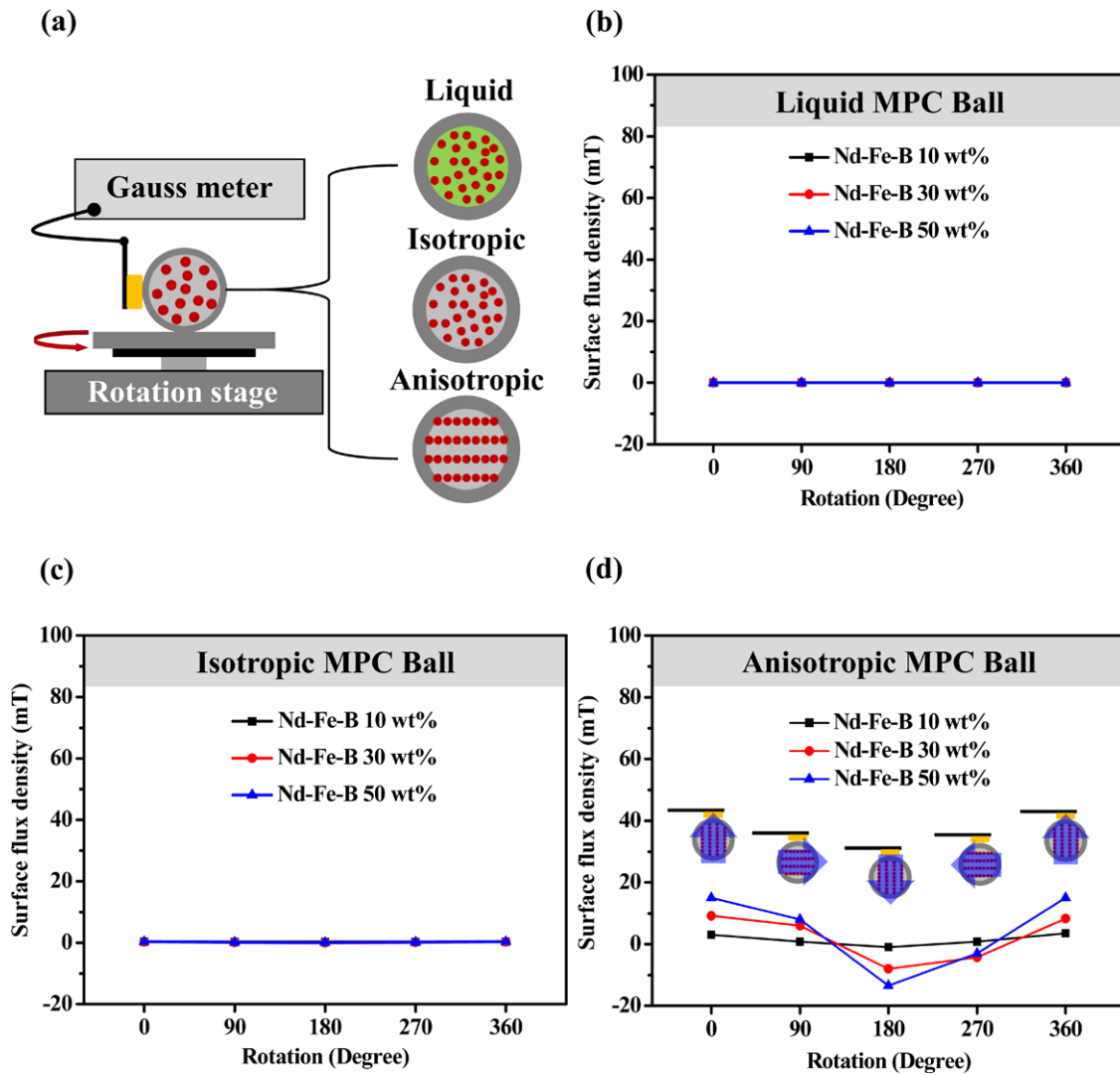


Figure 9. Measurements of the distribution of flux density for discrete MPC balls: (a) the measurement setup and the measurement results for discrete magnetic balls with (b) liquid MPC; (c), (d) solid magnetic isotropic and anisotropic MPCs of 10, 30 and 50 wt% NdFeB particles.

In comparison, the single fully solidified magnetic isotropic MPC layer ($3000\mu\text{m}$ in diameter and $500\mu\text{m}$ in thickness) is shown in figure 7(d). This device was implemented using the processes shown in figures 3(a)–(c). The distribution of the surrounding magnetic particles indicates the isotropic magnetic field. In addition, figure 7(e) shows a discrete component formed by the single surface-solidified magnetic anisotropic MPC layer. This discrete MPC component was fabricated on a glass substrate through the processes outlined in figure 3(a)–(c) and then removed from the substrate. This component has liquid MPC encapsulated by the solidified surface, as indicated in figure 3(f). The zoom-in micrograph in figure 7(f) shows the cross section of the discrete MPC component. The empty (since the liquid MPC was leaked out from the broken sample) solidified surface can be observed. Thus, the magnetic as well as the mechanical properties can be modulated by external magnetic fields. Moreover, the sample in figure 7(f) broke one month after it was fabricated. It indicates the long-term stability of

encapsulated liquid MPC at room temperature if there is no thermal curing agent.

4. Measurements and discussions

This study has performed various tests to characterize the magnetic properties of the fabricated micro MPC structures. Firstly the magnetic hysteresis loop (M–H curve) of the MPC balls were measured by using a VSM (vibrating sample magnetometer, Lake Shore 7407), as illustrated in figure 8(a). The micro balls (with a diameter of near $3000\mu\text{m}$) with liquid MPC, solid isotropic MPC and solid anisotropic MPC, as shown in figure 1(f), were characterized to determine their saturation magnetization, remanence and coercivity. The measurement results in figure 8(b) depict the M–H curves of the balls containing liquid MPC (the right-hand illustration in figure 1(f)) of three different wt% NdFeB particles (10 wt%, 30 wt% and 50 wt%). The saturation magnetization

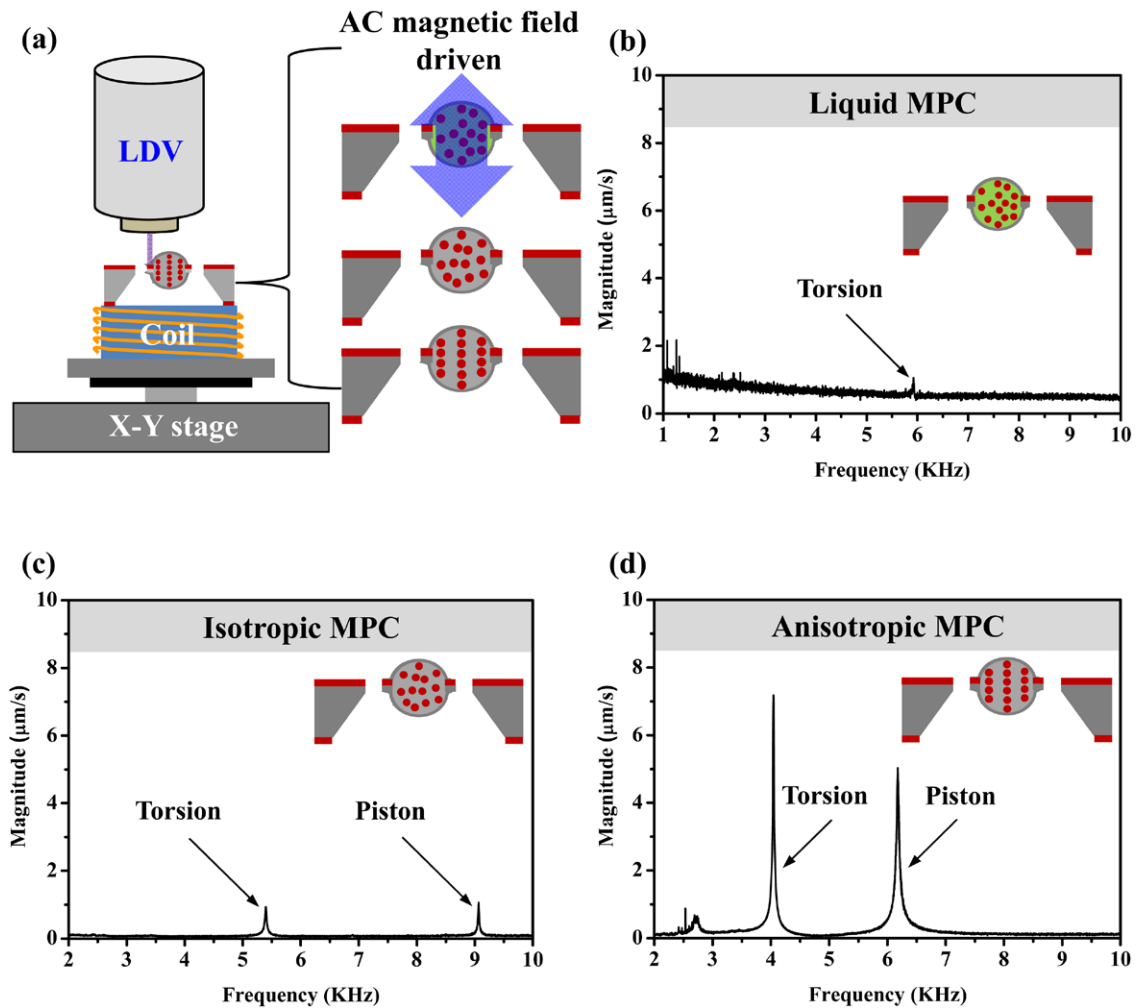


Figure 10. Dynamic tests on suspended MEMS structures integrated with different MPC balls: (a) the measurement setup and an inset to indicate the direction of magnetic driving force introduced by the coil and magnetic ball; and the dynamic responses of MEMS structure with (b) liquid MPC ball; (c), (d) solid magnetic isotropic and anisotropic MPC balls of 50 wt% NdFeB particles.

is increased with the wt% of NdFeB particles. It is noted that the measured magnetization of these balls changes abruptly after the applied magnetic field H slightly exceeds the coercivity. This characteristic is mainly due to the existence of liquid MPC. Thus, the randomly distributed NdFeB particles in the liquid polymer can be easily redistributed by the applied magnetic field and further increase the magnetization. Table 1 summarizes the measured saturation magnetization, remanence and coercivity of the micro balls with liquid MPC of different wt% NdFeB particles.

Measurements shown in figure 8(c) show the typical $M-H$ curves for the solidified magnetic isotropy MPC ball (the middle MPC ball in figure 1(f)) with 10 wt% NdFeB particles. In comparison, the measurements along two orthogonal axes of MPC balls (as indicated in figure 8(a)) are depicted with solid and dashed lines. Due to the magnetic isotropy of the MPC balls used in this test, identical $M-H$ curves were obtained for these two measurements. By comparing the $M-H$ curves in figures 8(b), (c), the coercivity of solidified magnetic isotropic MPC is higher than that of liquid MPC. Moreover, the magnetization of solidified magnetic isotropic MPC does not change drastically when the applied magnetic

field H exceeds the coercivity. These two differences are mainly caused by the constraint of the particle motion (linear or angular) in the applied magnetic field after polymer solidification. Measurements in figure 8(d) show the typical $M-H$ curves for the solidified magnetic anisotropy MPC ball (the left-hand MPC ball in figure 1(f)) with 10 wt% NdFeB particles. Similarly, the measurements parallel and orthogonal to the magnetization direction of the MPC ball are respectively depicted by the solid and dashed lines in figure 8(d). Due to the magnetic anisotropy of solidified MPC, the $M-H$ curves were different for these two measurement directions. Table 1 also summarizes the measured saturation magnetization, remanence and coercivity of the micro balls with isotropic and anisotropic solid MPC of different wt% NdFeB particles. The results indicate that anisotropic and isotropic solid MPCs of different powder concentrations have a constant coercivity. The coercivity of solid MPC is nearly one order of magnitude larger than that of the liquid MPC. In addition, the present process technologies enable the change of magnetic properties by varying with the wt% of the NdFeB particles and the alignment of the particles. However, the remanence and coercivity of the MPC implemented by the presented processes are

small as compared with the bulk materials (1200–1400 mT for remanence and 1000–1500 kA m⁻¹ for coercivity).

This study also established the test setup in figure 9(a) used to characterize the distribution of flux density for MPC balls using a Gauss meter. The magnetic ball was mounted on a rotation table and the Gauss meter was fixed on a stage. Thus, the flux density of the magnetic ball in different orientations was then recorded. Figures 9(b), (c) shows that the ball with liquid MPC has a small flux density of 0.01–0.02 mT, and that of the solidified isotropic MPC also has a small flux density of –0.03–0.3 mT, as the ball rotates from 0° to 360°. Moreover, the flux density of the ball with solidified anisotropic MPC varies from 15.1 mT to –13.1 mT for 50 wt% NdFeB (9 mT to –8.3 mT for 30 wt% NdFeB, and 2.4 mT to –1.5 mT for 10 wt% NdFeB) as the ball rotates from 0° to 180°. As shown in figure 10(a), the dynamic responses of the suspended MEMS structures respectively integrated with three different MPC balls of 50 wt% NdFeB particles have also been characterized by using a laser Doppler vibrometer (LDV). In this test, magnetic driving force (harmonic force) was applied on the MEMS structure through the MPC ball and the coil (with input AC current). Thus, the frequency of the driving force was modulated by the input AC current. Figures 10(b)–(d) shows the measured frequency responses of the three samples depicted in figure 10(a). Figure 10(b) indicates that the ball with liquid MPC could not introduce a sufficient magnetic force to drive the MEMS structure. It is expected that the periodic magnetic field from the coil only causes oscillation of the particles in the liquid polymer. As shown in figure 10(c), the resonant frequencies of the MEMS structure with a solid isotropic MPC ball could be observed. The first and second peaks respectively depict the first torsion mode and the first piston mode. Finally, the MEMS structure with a solid anisotropic MPC ball has the largest resonant peaks, as indicated in figure 10(d). This is due to the magnetization direction of the anisotropic MPC ball being coincident with the direction of driving force.

5. Conclusions

This study has implemented a two-stage solidification technology to realize micro magnetic structures using low temperature processes. UV-light polymer curing is used as the first stage of solidification to solidify the surface of the MPC structure. Thermal polymer curing is employed as the second stage of solidification to solidify the body of MPC. The distribution of magnetic particles in MPC can be specified by applying a magnetic field during the second solidification process. In addition, the micro structure with liquid MPC encapsulated by a solidified polymer surface can also be achieved if the liquid polymer has no thermal curing agent. In applications, the discrete MPC balls composed of 10–50 wt% of NdFeB particles with diameters ranging 500–3200 μm are demonstrated. These MPC balls respectively consist of liquid MPC encapsulated by a solid surface, solid isotropic MPC and solid anisotropic MPC. Furthermore, the integration of MPC structures on silicon substrate and

suspended MEMS devices has also been demonstrated. The magnetic performances of the fabricated MPC structures have also been characterized. Measurements indicate that a reasonable coercivity of 280 kA m⁻¹ was achieved for the solid MPC structure. In addition, the remanence and saturation magnetization of MPC can be improved by increasing the wt% of the magnetic particles. However, the remanence and saturation magnetization of the MPC implemented by the presented processes are still small as compared with the bulk materials.

Acknowledgements

This research is based on the work supported by National Science Council of Taiwan under grant number NSC-102-2221-E-007-027-MY3 and NSC-102-2622-E-007-014-MY3. The authors would like to express their appreciation to the Nano Facility Center at the National Chiao Tung University and the National Nano Device Laboratory for providing fabrication facilities.

References

- [1] Prados C, Hernando A, Hadjipanayis G C, Hadjipanayis G C and Gonzalez J M 1999 Coercivity analysis in sputtered Sm-Co thin films *J. Appl. Phys.* **85** 6148–50
- [2] Liakopoulos T M, Zhang W and Ahn C H 1996 Micromachined thick permanent magnet arrays on silicon wafers *IEEE Trans. Magn.* **32** 5154–6
- [3] Lagorce L K and Allen M G 1997 Magnetic and mechanical properties of micromachined strontium ferrite/polyimide composites *J. Microelectromech. Syst.* **6** 307–12
- [4] Lagorce L K, Brand O and Allen M G 1999 Magnetic microactuators based on polymer magnets *J. Microelectromech. Syst.* **8** 2–9
- [5] Niarchos D 2003 Magnetic MEMS: key issues and some applications *Sens. Actuators A* **106** 255–62
- [6] Arnold D P and Wang N 2009 Permanent magnets for MEMS *J. Microelectromech. Syst.* **18** 1255–66
- [7] Romero J J, Cuadrado R, Pina E, de Hoyos A, Pigazo F, Palomares F J, Hernando A, Sastre R and Gonzalez J M 2006 Anisotropic polymer bonded hard-magnetic film for microelectromechanical system application *J. Appl. Phys.* **99** 08N303
- [8] Wang N, Bowers B J and Arnold D P 2008 Wax-bonded NdFeB micromagnets for microelectromechanical systems applications *J. Appl. Phys.* **103** 07E109
- [9] Damean N, Parviz B A, Lee J N, Odom T and Whitesides G M 2005 Composite ferromagnetic photoresist for the fabrication of microelectromechanical systems *J. Micromech. Microeng.* **15** 29–34
- [10] Dutoit B M, Besse P-A, Blanchard H, Guerin L and Popvi R S 1999 High performance micromachined Sm₂Co₁₇ polymer bonded magnets *Sens. Actuators A* **77** 178–182
- [11] Kim J, Chung S E, Choi S-E, Lee H, Kim J and Kwon S 2011 Programming magnetic anisotropy in polymeric microactuators *Nat. Mater.* **10** 747–52
- [12] Kobayashi K and Ikuta K 2009 3D magnetic microactuator made of newly developed magnetically modified photocurable polymer and application to swimming micromachine and microscrew pump *Proc. 22nd Int. Conf. MEMS (Sorrento, Jan. 2009)* pp 11–4

- [13] Endruweit A, Johnson M S and Long A C 2006 Curing of composite components by ultraviolet radiation: a review *Polym. Compos.* **27** 119–28
- [14] Carlson J D and Jolly M R 2000 MR fluid, foam and elastomer devices *Mechatronics* **10** 555–69
- [15] Park B J, Fang F F and Choi H J Magnetorheology: materials and application *Soft Matter* **6** 5246–53
- [16] Park S Y, Handa H and Sandhu A 2010 Magneto-optical biosensing platform based on light scattering from self-assembled chains of functionalized rotating magnetic beads *Nano Lett.* **10** 446–51
- [17] Wen W, Ma H, Tam W Y and Sheng P 1998 Anisotropic dielectric properties of structured electroheological fluids *Appl. Phys. Lett.* **73** 3070–2
- [18] Jolly M R, Carlson J D and Munoz B C 1996 A model of the behaviour of magnetorheological materials *Smart Mater. Struct.* **5** 607–14
- [19] Zhu H, Zhang C, Liu S, Tang Y and Yin Y 2006 Effects of nanoparticle clustering and alignment on thermal conductivities of Fe₃O₄ aqueous nanofluids *Appl. Phys. Lett.* **89** 023123
- [20] Majidi C and Wood R J 2010 Tunable elastic stiffness with microconfined magnetorheological domains at low magnetic field *Appl. Phys. Lett.* **97** 164104
- [21] Hsu F-M, Chen W-C, Hu C-F, Liu G-Y and Fang W 2013 Formation and integration of tunable anisotropic magnetic polymer composites by two stages solidification process *Proc. 17th Int. Conf. Solid-State Sensors, Actuators and Microsystems (Transducers and Eurosensors XXVII) (Barcelona, Jun. 2013)* pp 2672–5
- [22] Hsu F-M, Chen W-C, Lai W-M and Fang W 2014 Implementation of single/multi-layer magnetic-anisotropy magnetic polymer composites for magnetic property modulation *Proc. IEEE 27th Int. Conf. MEMS (San Fransisco, CA, Jan. 2014)* pp 44–7
- [23] Lee C C, Hsiao S Y and Fang W 2009 Formation and integration of a ball lens utilizing two phase liquid technology *Proc. 22nd IEEE Int. Conf. MEMS (Sorrento, Jan. 2009)* pp 172–5
- [24] Hsiao S Y, Lee C C and Fang W 2008 The implementation of concave micro optical devices using a polymer dispensing *J. Micromech. Microeng.* **18** 085009